On Cagniard's problem for a *qSH* line source in transversely isotropic media*

Lawrence H. T. Le

ABSTRACT

The paper studies the response to a *qSH*–pulse generated by a line source, of two homogeneous half-spaces (transversely isotropic elastic or viscoelastic) separated by a plane boundary.

For a simple model of two transversely isotropic half-spaces in welded contact, all the arrivals including the incident, reflected, head, transmitted and evanescent waves, that are predicted by the isotropic theory, are present. For the 15% change in wave speeds considered here, anisotropy changes the dynamic and kinematic characteristics of the pulses. Depending on the anisotropy factor, the change can be pronounced. Because of the significant time shift and amplitude variation of the first arrivals due to anisotropy, proper consideration of the anisotropy of the medium is necessary in interpreting vertical seismic profiles or crosshole seismic data by means of any travel time or amplitude tomographic scheme.

INTRODUCTION

A medium consisting of homogeneous isotropic layers with flat interfaces will appear as a transversely isotropic medium with a vertical axis of symmetry at wavelengths longer than the layer thickness (Postma, 1955). We consider here the problem of a *qSH*–pulse generated by a line source acting in a model consisting of two homogeneous and transversely isotropic (TI) half-spaces in welded contact along a plane boundary. A treatment of the isotropic (I) case was examined most recently by Abramovici et al. (1989 and 1990). Sato and Lapwood (1968) treated the case of *SH*-waves in a transradially isotropic cylinder.

We start by presenting the Cagniard-de Hoop solutions for two half-spaces. This is followed by solutions in wavenumber-frequency $(\omega$–$k)$ space so that results calculated by two different methods can be compared for accuracy. Synthetic seismograms for various models are then discussed.

THE CAGNIARD–DE HOOP SOLUTIONS

Let a right-handed Cartesian coordinate system be oriented so that the positive z-axis faces downward (Fig. 1). Two homogeneous and transversely isotropic half-spaces characterized by densities ρ_i and elastic constants, L_i, N_i $(i = 1,2)$ are welded along the (x,y) plane. A line source generating *qSH*-waves is located along the y-axis

* will appear in the *Bulletin of Seismological Society of America, 1993.*

at a height, $-z_o$ ($z_o>0$). The differential equations governing the particle displacement v everywhere are

$$\rho_j \frac{\partial^2 v_j}{\partial t^2} - N_j \frac{\partial^2 v_j}{\partial x^2} - L_j \frac{\partial^2 v_j}{\partial z^2} = \delta(x)\,\delta(z+z_o)\,\delta(t) \qquad (j=1,2) \tag{1}$$

subjected to the initial conditions $v = \frac{\partial v}{\partial t} = 0$ for $t = 0$, the radiation condition and the boundary conditions at the interface, $z=0$:

$$v_1 = v_2 \quad , \quad L_1 \frac{\partial v_1}{\partial z} = L_2 \frac{\partial v_2}{\partial z} \quad . \tag{2}$$

When the receiver is in the upper half-space, we have

$$v_1 = v_d + v_r + v_h \tag{3}$$

where the subscripts denote direct *(d)*, reflected *(r)* and head *(h)* waves respectively. By using the Cagniard-de Hoop method (de Hoop, 1960; Drijkoningen and Chapman, 1988; Abramovici et al., 1989), the direct arrival is:

$$v_d(x,z,t) = \frac{1}{2\pi\sqrt{N_1 L_1}} \frac{\mathrm{H}\left(t - \frac{r}{(\beta_h)_1}\right)}{\sqrt{t^2 - \frac{r^2}{(\beta_h^2)_1}}} \quad , \tag{4}$$

where $H(t)$ is the Heaviside step function,

$$r = \sqrt{x^2 + \frac{N_1}{L_1}|z+z_o|^2} \quad . \tag{5}$$

and the horizontal wave speed is

$$\beta_h = \sqrt{\frac{N}{\rho}} \quad . \tag{6}$$

It is also convenient at this point to define the vertical wave speed as

$$\beta_v = \sqrt{\frac{L}{\rho}} \quad . \tag{7}$$

The reflected wave is

$$v_r(x,z,t) = \frac{1}{2\pi\sqrt{N_1 L_1}} \mathrm{Re}\left(\frac{L_1\eta_1 - L_2\eta_2}{L_1\eta_1 + L_2\eta_2}\right) \frac{\mathrm{H}\left(t - \frac{r_1}{(\beta_h)_1}\right)}{\sqrt{t^2 - \frac{r_1^2}{(\beta_h^2)_1}}} \tag{8}$$

for $t > \frac{r_1}{(\beta_h)_1}$. The head wave , if it exists, is

$$v_h(x,z,t) = -\frac{1}{2\pi\sqrt{N_1 L_1}} \mathrm{Im}\left(\frac{L_1\eta_1 - L_2\eta_2}{L_1\eta_1 + L_2\eta_2}\right) \frac{\mathrm{H}(t - t_h)}{\sqrt{\frac{r_1^2}{(\beta_h^2)_1} - t^2}} \tag{9}$$

for $t_h < t < \frac{r_1}{(\beta_h)_1}$ where Re[...] and Im[...] denote the real and imaginary parts of a complex quantity,

$$\eta_j(\zeta) = \sqrt{\frac{N_j}{L_j}} \sqrt{\frac{1}{(\beta_h^2)_j} - \zeta^2} \quad , \quad \mathrm{Re}(\eta_j) \geq 0 \quad (j = 1, 2), \tag{10}$$

and

$$r_1 = \sqrt{x^2 + \frac{N_1}{L_1}|z - z_o|^2} \quad . \tag{11}$$

The arrival time, t_h of the head wave is

$$t_h = \frac{x}{(\beta_h)_2} + |z - z_o| \sqrt{\frac{N_1}{L_1}} \sqrt{\frac{1}{(\beta_h^2)_1} - \frac{1}{(\beta_h^2)_2}} \quad , \tag{12}$$

the critical distance, x_c is

$$x_c = \sqrt{\frac{N_1}{L_1}} |z - z_o| \tan\theta_c \ , \tag{13}$$

where θ_c is the critical auxiliary angle

$$\sin\theta_c = \frac{(\beta_h)_1}{(\beta_h)_2} \ , \tag{14}$$

and the quantity ζ at any given time t in expression (10) is given, respectively, by

$$\zeta = \begin{cases} \dfrac{-t\,x + \sqrt{\dfrac{N_1}{L_1}}\,|z - z_o|\sqrt{\dfrac{r_1^2}{(\beta_h^2)_1} - t^2}}{r_1^2} & t_h < t < \dfrac{r_1}{(\beta_h)_1} \\ \dfrac{-t\,x + i\sqrt{\dfrac{N_1}{L_1}}\,|z - z_o|\sqrt{t^2 - \dfrac{r_1^2}{(\beta_h^2)_1}}}{r_1^2} & t > \dfrac{r_1}{(\beta_h)_1} \end{cases} , \tag{15}$$

where $i^2 = -1$.

When the receiver is in the other half-space, the transmitted particle displacement is

$$v_t = -\frac{1}{2\pi L_1} \mathrm{H}(t - t_o)\ \mathrm{Im}\left\{ \frac{T}{\eta_1} \frac{1}{x + \dfrac{N_1}{L_1}\dfrac{z_o\,\zeta}{\eta_1(\zeta)} + \dfrac{N_2}{L_2}\dfrac{z\,\zeta}{\eta_2(\zeta)}} \right\}_{\tau_t = t} \tag{16}$$

where T is the transmission coefficient:

$$T = \frac{2L_1\eta_1}{L_1\eta_1 + L_2\eta_2} , \tag{17}$$

$$\tau_t = -\zeta x + \eta_1 z_o + \eta_2 z , \tag{18}$$

and ζ is the solution of the implicit equation (18) given $\tau_t = t$. The arrival time t_o of the transmitted wave is given by (18) at $z = z_o$ where z_o is the negative root of the equation

$$\frac{\sqrt{\dfrac{N_1}{L_1}}\,z_o\,\zeta_o}{\sqrt{\dfrac{1}{(\beta_h^2)_1} - \zeta_o^2}} + \frac{\sqrt{\dfrac{N_2}{L_2}}\,z\,\zeta_o}{\sqrt{\dfrac{1}{(\beta_h^2)_2} - \zeta_o^2}} = -x . \tag{19}$$

When $N = L$ $(= \mu)$, the solutions reduce to the isotropic solutions .

THE SOLUTIONS IN ω–k INTEGRALS

The solutions given by Eqns. (4), (8), (9) and (16) are the Green's functions. The functions can be convolved with a band-limited source function, say, $g(t)$, to simulate a realistic response. The solutions can be obtained by a different route using the Fourier transform. Following the procedure presented by Abramovici et al. (1990), the convolved solution, $\hat{v}$, of the problem for $z < 0$ is:

$$\hat{v}_1 = \frac{f_o}{8\pi^2 L_1} \int_{-\infty}^{\infty} G(\omega)\, e^{i\omega t}\, d\omega \int_{-\infty}^{\infty} \frac{1}{\hat{\eta}_1} \left[e^{-\hat{\eta}_1 |z + z_o|} + \frac{L_1\hat{\eta}_1 - L_2\hat{\eta}_2}{L_1\hat{\eta}_1 + L_2\hat{\eta}_2}\, e^{\hat{\eta}_1 (z - z_o)} \right] e^{-ikx}\, dk \tag{20}$$

and for $z > 0$:

$$\hat{v}_2 = \frac{f_o}{8\pi^2 L_1} \int_{-\infty}^{\infty} G(\omega)\, e^{i\omega t}\, d\omega \int_{-\infty}^{\infty} \frac{2\, L_1}{L_1\hat{\eta}_1 + L_2\hat{\eta}_2}\, e^{-\hat{\eta}_1 z_o - \hat{\eta}_2 z}\; e^{-ikx}\, dk \quad , \tag{21}$$

where f_o is the force per unit length, per unit time, $G(\omega)$ is the Fourier transform of the source function $g(t)$ and

$$\hat{\eta}_j = \sqrt{\frac{N_j}{L_j}} \begin{cases} \sqrt{k^2 - \dfrac{\omega^2}{(\beta_h^2)_j}} & \text{if } |k| > \left|\dfrac{\omega}{\beta_h}\right| \\ i\sqrt{\dfrac{\omega^2}{(\beta_h^2)_j} - k^2} & \text{if } |k| < \left|\dfrac{\omega}{\beta_h}\right| \end{cases} \qquad (j = 1, 2)\ . \tag{22}$$

Absorption can be introduced into the media by making the velocities complex via the Azimi's law (Abramovici at al., 1990).

DISCUSSION OF THE RESULTS

For comparison, we have chosen a TI model having β_v 10% less than β_h (anisotropy factor $F_3 = \beta_h / \beta_v = 1.11$) : $(\beta_h)_1$ and $(\beta_v)_1$ are 1.0 km/sec and 0.9 km/sec for the upper half-space while $(\beta_h)_2$ and $(\beta_v)_2$ are 2.4 km/sec and 2.16 km/sec for the lower half-space. The density ratio is $\rho_1{:}\rho_2$ = 1:2. We worked with nondimensional quantities, the scaling factors, $\bar{\beta}$ for velocity, $\bar{\rho}$ for density, and $\bar{l}$ for length being 2 km/sec, 2000 kg/m^3 and 5 m, respectively. The source wavelet used to simulate the particle velocity is the derivative of a Gaussian function with dominant frequency of 50 Hz (Abramovici et al., 1989 and 1990). Figure 2 compares the results for a receiver located in the same half-space as the source (Fig. 2a) and in the other half-space (Fig. 2b). A cosine taper (0/5/230/250 Hz) has been applied to the ω-k seismograms. The good comparison confirms that the solutions [Eqns. (4), (8), (9), (16), (20) & (21)] derived by using two different methods and numerical techniques are correct.

Figure 3 displays the results for an I/TI model. An I/I model is used as reference having $(\beta_h)_1 = (\beta_v)_1$ = 1 km/s and $(\beta_h)_2 = (\beta_v)_2$ = 2.4 km/sec. The density ratio is $\rho_1{:}\rho_2$ = 1:2. The I/TI models are obtained by changing $(\beta_v)_2$ while keeping the isotropic upper half space and $(\beta_h)_2$ unchanged. Since the arrival times of

the phases (incident, reflected and head waves) in the upper half-space depend on the elastic constants of that half-space and $(\beta_h)_2$, the phases have the same arrival time in all cases (Fig. 3a). However, for the ±15% change in vertical wave speed in the lower half-space, the effect on the reflection coefficient is minute as seen from the amplitudes of the reflected and head waves. The incident ray angle ϕ for the reflected wave is 51.3° and the correspondent incident phase angles θ , obtained from the ray angle using $\tan\theta = \left(\frac{\beta_v}{\beta_h}\right)^2 \tan\phi$ [see, e.g., Byun, 1982], are 42.0° and 59.0° for $(F_3)_2$ = 1.18 and 0.87, respectively. Since the receiver in the lower half-space is located near the interface (3 m away), the ray path for the transmitted arrival is controlled strongly by the horizontal wave speed. This is indeed seen on Figure 3b. The transmitted amplitude decreases by a small amount when $(F_3)_2$ increases from 0.87 to 1.18. Even though the direction of energy leakage of the evanescent wave is vertical (Abramovici et al., 1989), the ±15% change in vertical wave speed does not alter its amplitude significantly. No obvious time shift of the evanescent arrivals occurs in this case. For our next I/TI model we held $(\beta_v)_2$ = 2.4 km/s constant and increased $(\beta_h)_2$ by ±15% of $(\beta_v)_2$. The head wave (Fig. 4a) which travels horizontally in the lower medium with $(\beta_h)_2$ is advanced 9 msec for $(F_3)_2$ = 1.15 and delayed 11 msec for $(F_3)_2$ = 0.85 as compared to the isotropic case. We attribute the change in amplitude of the head wave mainly to the fact that the head wave of positive polarity rests on the negative "tail" of the incident arrival, rather than to the impedance contrast. The transmitted arrival (see Fig. 4b) which travels almost horizontally in the lower medium is advanced 11.3 msec for $(F_3)_2$ = 1.15 and delayed 14.6 msec for $(F_3)_2$ = 0.85. The transmitted amplitude increases by 15% and the evanescent amplitude almost doubles when $(F_3)_2$ drops from 1.15 to 0.85.

Figure 5 shows the results for a TI/I model where the upper half-space is TI and the line source generates the *qSH* wave disturbance. In this case, the lower isotropic half-space has $(\beta_h)_2 = (\beta_v)_2$ = 2.4 km/s and $(\beta_h)_1$ = 1 km/s is held constant. The incident waves (see Fig. 5a) arrive at the same time for all cases, since the source and the receiver are at the same level and the difference in amplitude is due to the change of the elastic constant L1 via Eqn. (7). The reflected amplitude increases approximately by 25% when $(F_3)_1$ increases from 0.87 to 1.18; the transmitted wave (see Fig. 5b) decreases by 5%. However, the difference in the transmitted arrival times is as great as 28 msec between $(F_3)_1$ = 0.87 and 1.18. The evanescent wave suffers a time shift without obvious change in amplitude. Figure 6 considers the case where $(\beta_v)_1$ is fixed while changing $(\beta_h)_1$. The incident arrivals are time-shifted as expected (see Fig. 6a). The incident and head waves arrive approximately at the same time (t_d = 0.294 sec and t_h = 0.291 sec) for $(F_3)_1$ = 0.85 and interfere constructively to amplify the positive incident peak. The evanescent wave is advanced in time and approximately doubles in amplitude as $(F_3)_1$ increases from 0.85 to 1.15 (Fig. 6b).

Figure 7A shows synthetic seismograms for a horizontal array of receivers. The source and the receivers are at the same level of 100 m above the interface. The isotropic model used has β_1 = 0.85 km/s and β_2 = 1.7 km/s and the TI model has $(\beta_v)_1$ = 0.85 km/s, $(\beta_v)_2$ = 1.7 km/s, $(\beta_h)_1$ = 1 km/s and $(\beta_h)_2$ = 2 km/s [$(\beta_v)_1$: $(\beta_v)_2 = (\beta_h)_1 : (\beta_h)_2 = \rho_1 : \rho_2 = 1 : 2$]. Only the reflected amplitudes are computed. The ray angle spans from 3° to 51° and the phase angle from 2° to 42° correspondingly

for the TI model. The critical distance is 115.5 m for the isotropic model and 135.9 m for the TI model. The picked amplitudes are shown in Figure 7B. The relative changes of arrival times and amplitudes with respect to the isotropic results are shown in Figure 7C. The relative change is calculated by dividing the time difference $T_{TI} - T_I$ or the amplitude difference $Amp_{TI} - Amp_I$, by T_I or Amp_I. In this manner, the relative change for the same difference depends on the magnitude of the denominator and is more pronounced for events which arrive earlier and have low amplitude. In Figure 7C, the amplitude versus offset (AVO) experiences an average of 14% difference for the precritical arrivals while the arrival time has an approximately linear change as expected. Figure 8A is a vertical seismic profile (VSP) with offset at 100 m. Only the incident and transmitted arrivals are calculated. The picked amplitudes are shown in Figure 8B with the relative changes in Figure 8C. The amplitude has an average of 9% change. The arrival time suffers the largest change of 14% when the ray almost travels horizontally (i.e., $z = -115$, -100 and -85 m) since the maximum difference in the wave speeds (TI versus isotropic) is along the horizontal direction.

CONCLUSION

The Cagniard's problem for the propagation of *SH*-waves in transversely isotropic media is solved by the Cagniard-de Hoop method and by the ω–k method. The solutions thus derived are similar to those for isotropic media except that the vertical coordinate is scaled by the square root of the ratio of elastic constants, .

For the 15% anisotropy considered in this paper, the time shift and AVO effect are significant as compared to the isotropic case. Any inversion scheme which neglects the existence of anisotropy of the media will tend to yield erroneous solution.

ACKNOWLEDGMENTS

This research was supported by the Consortium for Research in Elastic Wave of Exploration Seismology (the CREWES project). All the computation was performed using the Sun Sparc stations and Myrias Parallel machine (SPS-2) at the University of Calgary. I thank Dr. David Eaton of ARCO who raised a question which led to the formulation of the problem and Dr. Bok S. Byun of ARCO for the reprints on elliptical anisotropy. Profs. Flavian Abramovici and Ed Krebes have given critical comments. The model for Figures 7 and 8 was suggested by Don Lawton.

REFERENCES

Abramovici, F., Le, L. H. T. and Kanasewich, E. R., 1989, The evanescent wave in Cagniard's problem for a line source generating SH waves: Bull. Seism. Soc. Am., 79, 1941-1955.

Abramovici, F., Le, L. H. T. and Kanasewich, E. R., 1990, The solution of Cagniard's problem for a SH line source in elastic and anelastic media, calculated using ω-k integrals: Bull. Seism. Soc. Am., 80, 1297-1310.

Aki, K. and Richards, P. G., 1980, Quantitative Seismology, vol. 1, W. H. Freeman and Co., San Francisco, California.

Byun, B. S., 1982, Seismic parameters for media with elliptical velocity dependencies: Geophysics, 47, 1621-1626.

de Hoop, A. T., 1960, A modification of Cagniard's method for solving seismic pulse problems: Appl. Sci. Res., B8, 349-356.

Drijkoningen, G. G. and Chapman, C. H., 1988, Tunneling rays using the Cagniard-de Hoop method: Bull. Seism. Soc. Am., 78, 898-907.

Postma, G. W., 1955, Wave propagation in a stratified medium: Geophysics, 20, 780-806.

Sato, R. and Lapwood, E. R., 1968, *SH* waves in a transversely-isotropic medium – II Transradially isotropic cylinder: Geophys. J. R. astr. Soc., 16, 461-473.

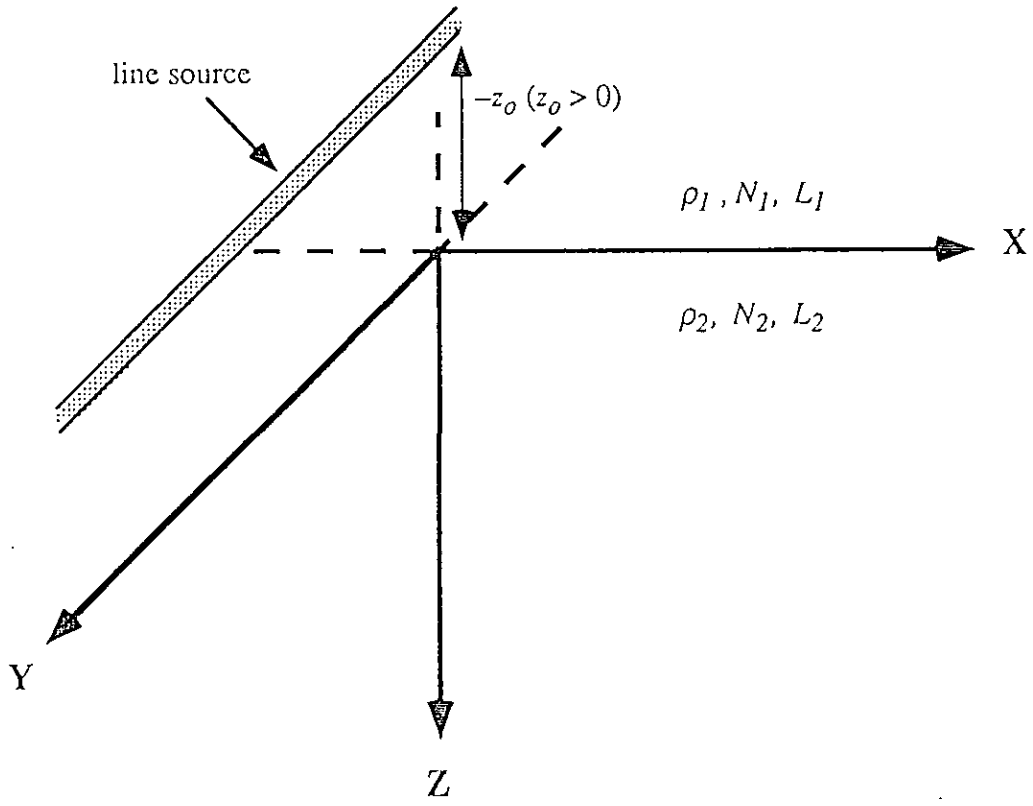

Figure 1: (a) A line source of unit length along the y-axis at a height $-z_o$ generating the qSH-waves and the geometry of the model.

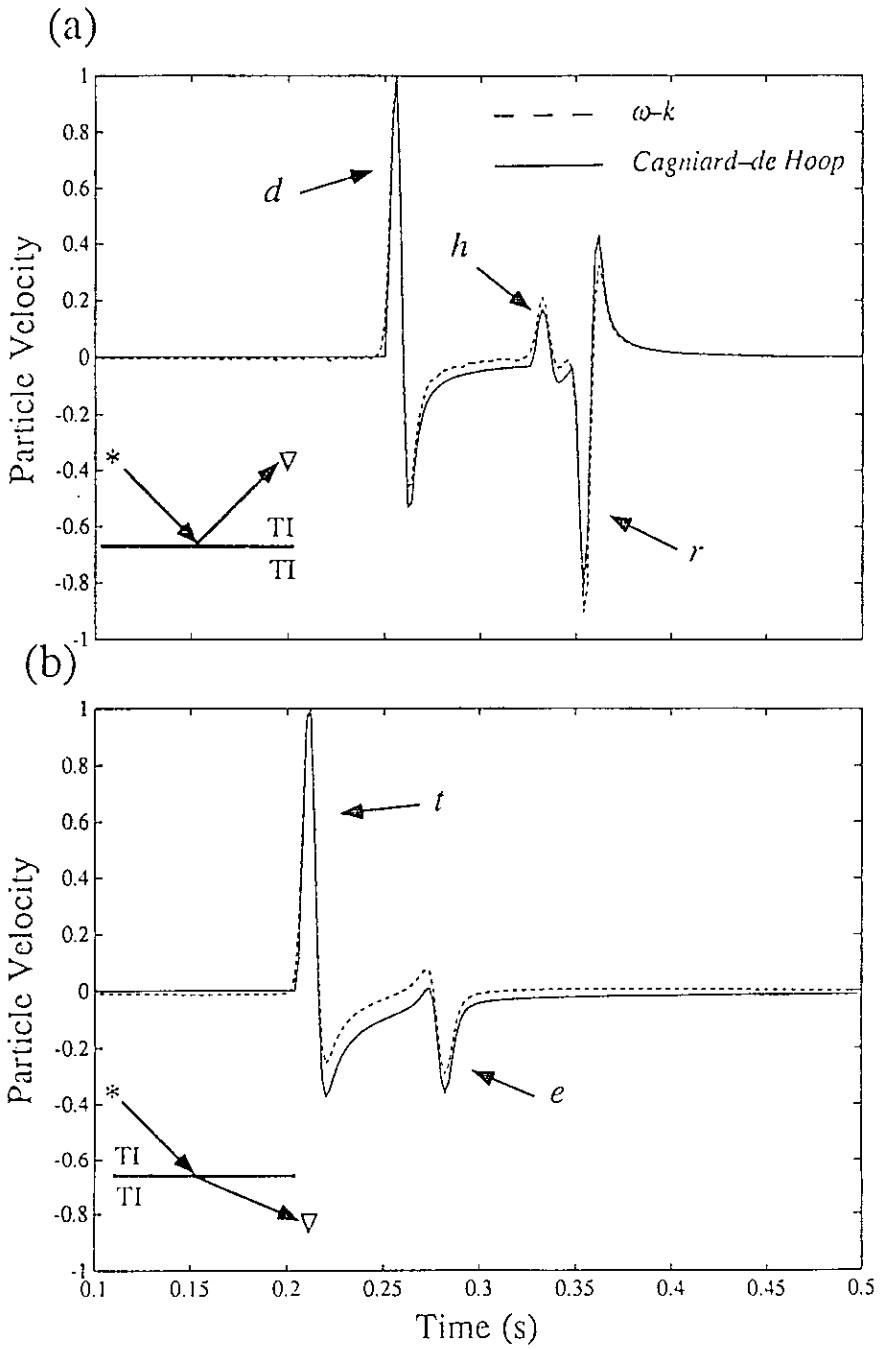

Figure 2: Comparison of the results computed by two different methods for an elastic TI structure. The anisotropy factor, F_3, is 1.11 for both half-spaces: $(\beta_h)_1$ and $(\beta_v)_1$ being 1.0 km/sec and 0.9 km/sec for the upper half-space and $(\beta_h)_2$ and $(\beta_v)_2$ being 2.4 km/sec and 2.16 km/sec for the lower half-space. The density ratio is $\rho_1:\rho_2$ = 1:2. (a) The receiver is in the same half-space as the source (z_o = 100 m, x = 250 m and z = −120 m). (b) The receiver is in the other half-space (z = 3 m). The direct, reflected, head wave, transmitted and evanescent arrivals are, respectively, denoted as *d*, *r*, *h*, *t*, and *e*. (*) denotes the source and (∇) denotes the receiver.

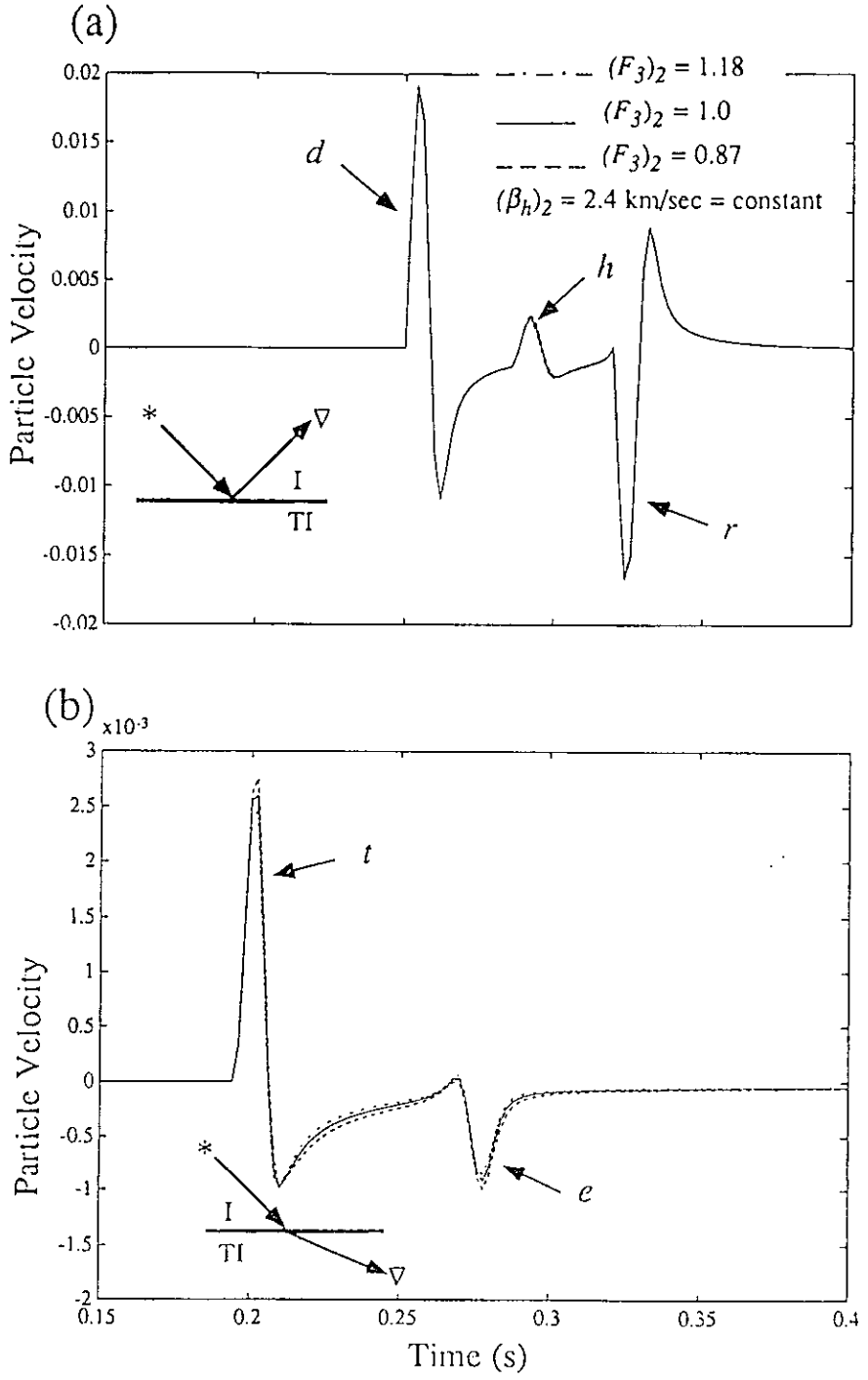

Figure 3: Comparison of I/I (solid) and I/TI (dashed and dash-dotted) results obtained by the Cagniard-de Hoop method. (a) The receiver is in the same half-space as the source (z_o = 100 m, x = 250 m and z = –100 m). (b) The receiver is in the other half-space (z = 3 m). The direct, reflected, head wave, transmitted and evanescent arrivals are, respectively, denoted as *d*, *r*, *h*, *t*, and *e*. (*) denotes the source and (∇) denotes the receiver. The anisotropy factor for the two TI lower half-spaces are $(F_3)_2$ = 1.18 (dash-dotted) and 0.87 (dashed) respectively while keeping $(\beta_h)_2$ = 2.4 km/sec constant.

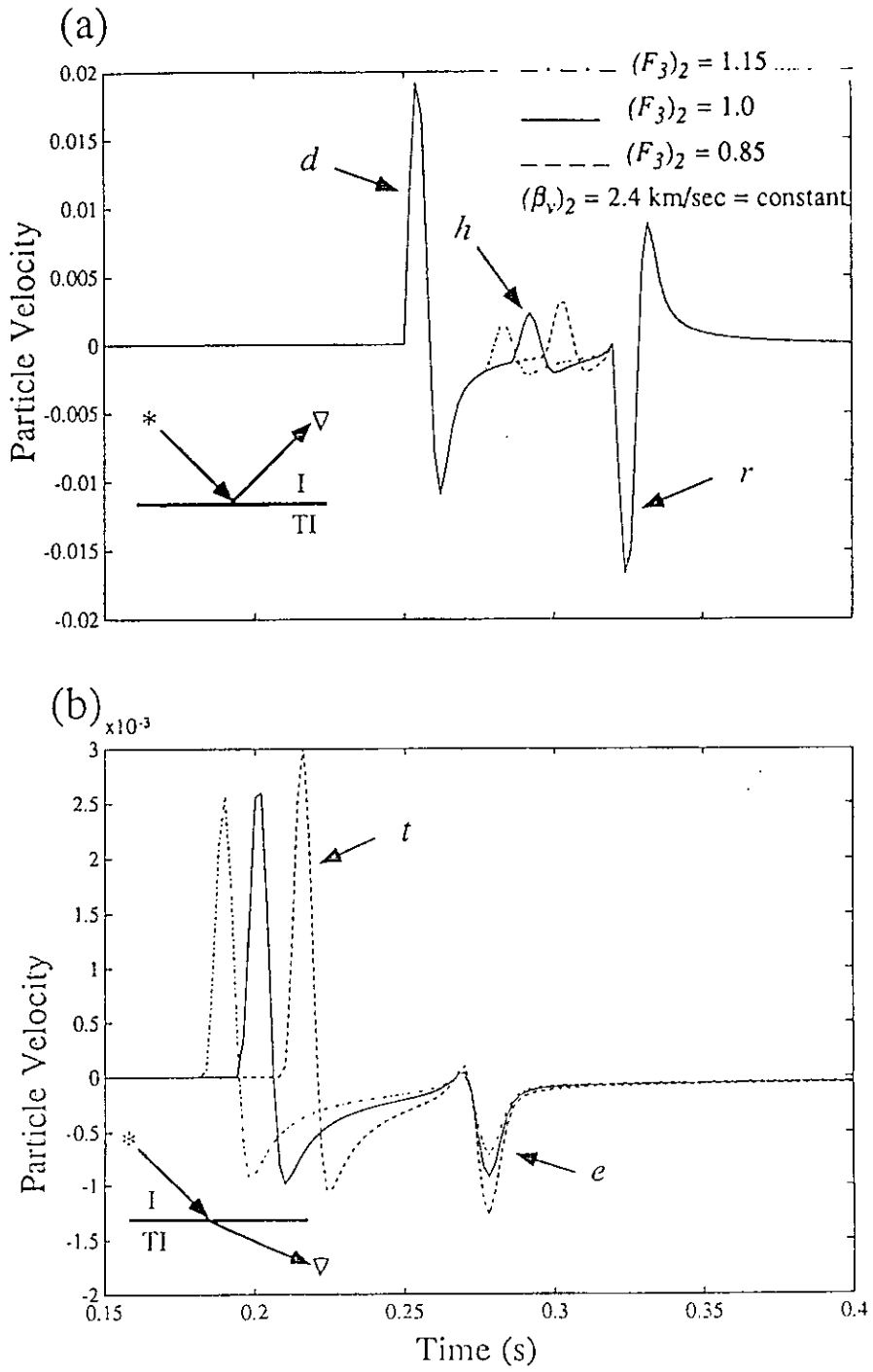

Figure 4: Comparison of I/I (solid) and I/TI (dashed and dash-dotted) results obtained by the Cagniard-de Hoop method. (a) The receiver is in the same half-space as the source (z_o =100 m, x = 250 m and z = –100 m). (b) The receiver is in the other half-space (z = 3 m). The direct, reflected, head wave, transmitted and evanescent arrivals are, respectively, denoted as *d*, *r*, *h*, *t*, and *e*. (*) denotes the source and (∇) denotes the receiver. The anisotropy factor for the two TI lower half-spaces are $(F_3)_2$ = 1.15 (dash-dotted) and 0.85 (dashed) respectively while keeping $(\beta_v)_2$ = 2.4 km/sec constant.

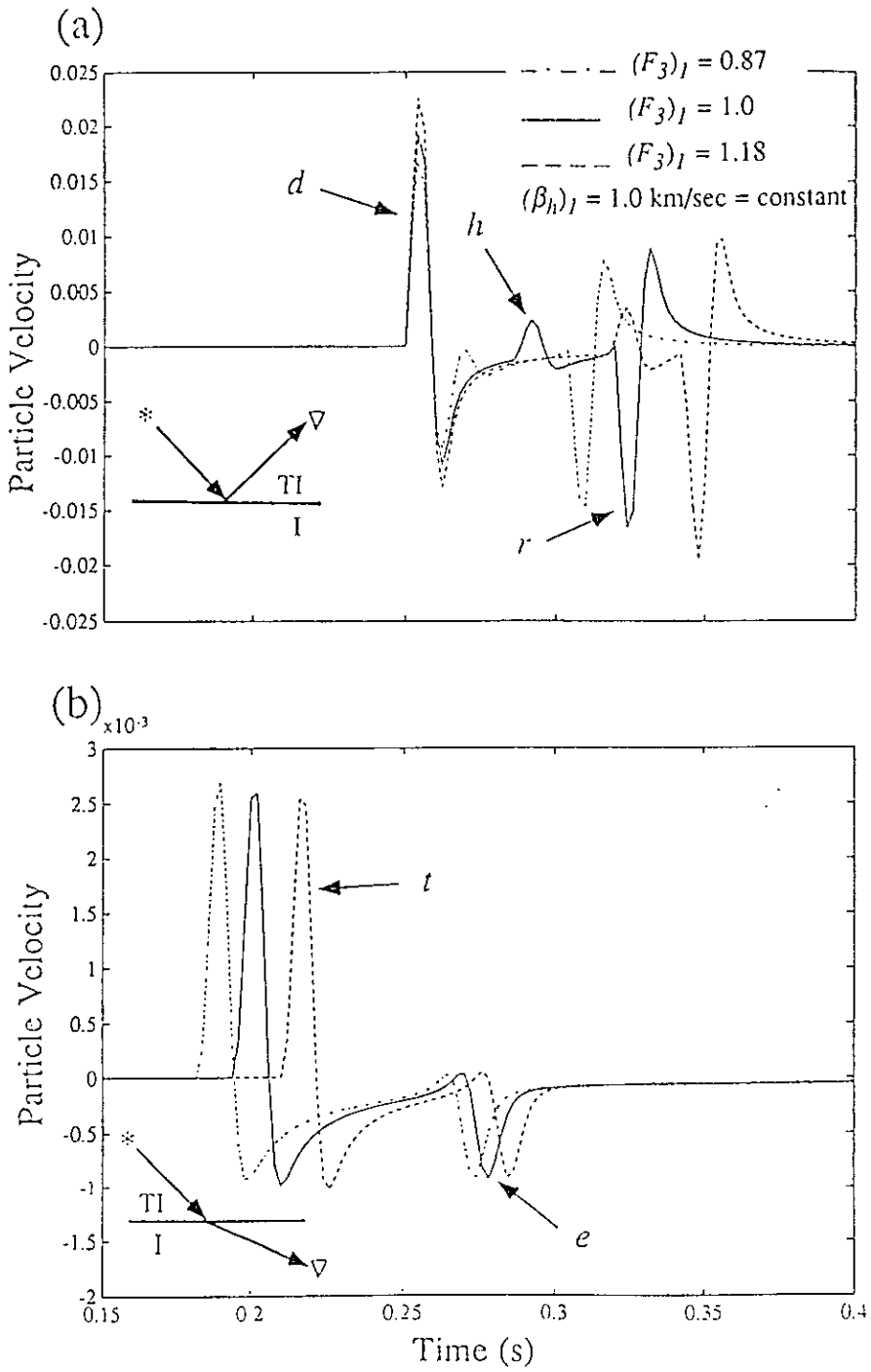

Figure 5: Comparison of I/I (solid) and TI/I (dashed and dash-dotted) results obtained by the Cagniard-de Hoop method. (a) The receiver is in the same half-space as the source (z_o = 100 m, x = 250 m and z = –100 m). (b) The receiver is in the other half-space (z = 3 m). The direct, reflected, head wave, transmitted and evanescent arrivals are, respectively, denoted as *d*, *r*, *h*, *t*, and *e*. (*) denotes the source and (∇) denotes the receiver. The anisotropy factor for the two TI upper half-spaces are $(F_3)_I$= = 0.87 (dash-dotted) and 1.18 (dashed) respectively while keeping $(\beta_h)_I$ = 1.0 km/sec constant.

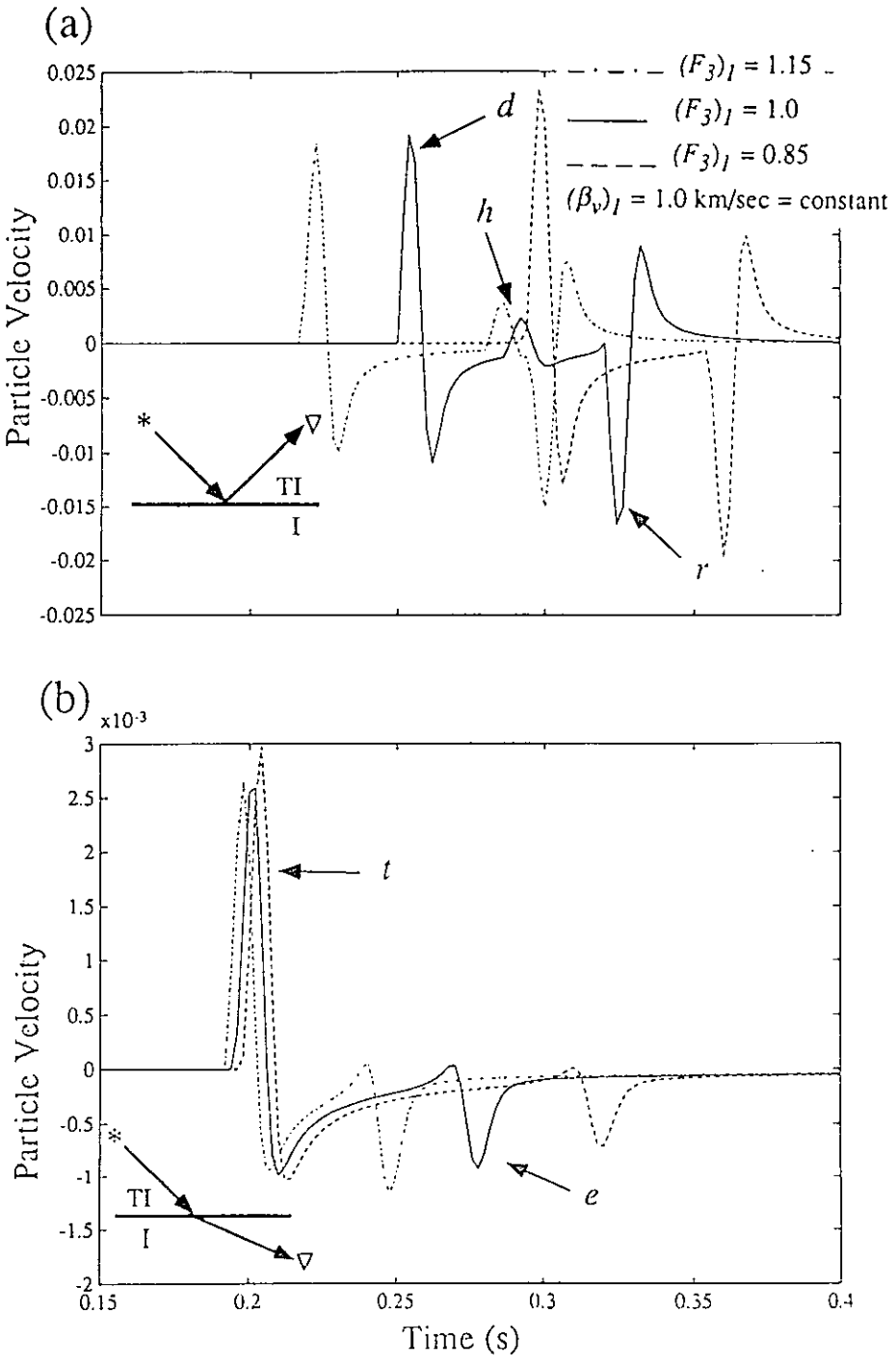

Figure 6: Comparison of I/I (solid) and TI/I (dashed and dash-dotted) results obtained by the Cagniard-de Hoop method. (a) The receiver is in the same half-space as the source (z_o = 100 m, x = 250 m and z = –100 m). (b) The receiver is in the other half-space (z = 3 m). The direct, reflected, head wave, transmitted and evanescent arrivals are, respectively, denoted as *d*, *r*, *h*, *t*, and *e*. (*) denotes the source and (∇) denotes the receiver. The anisotropy factor for the two TI upper half-spaces are $(F_3)_1$ = 1.15 (dash-dotted) and 0.85 (dashed) respectively while keeping $(\beta_v)_1$ = 1.0 km/sec constant.

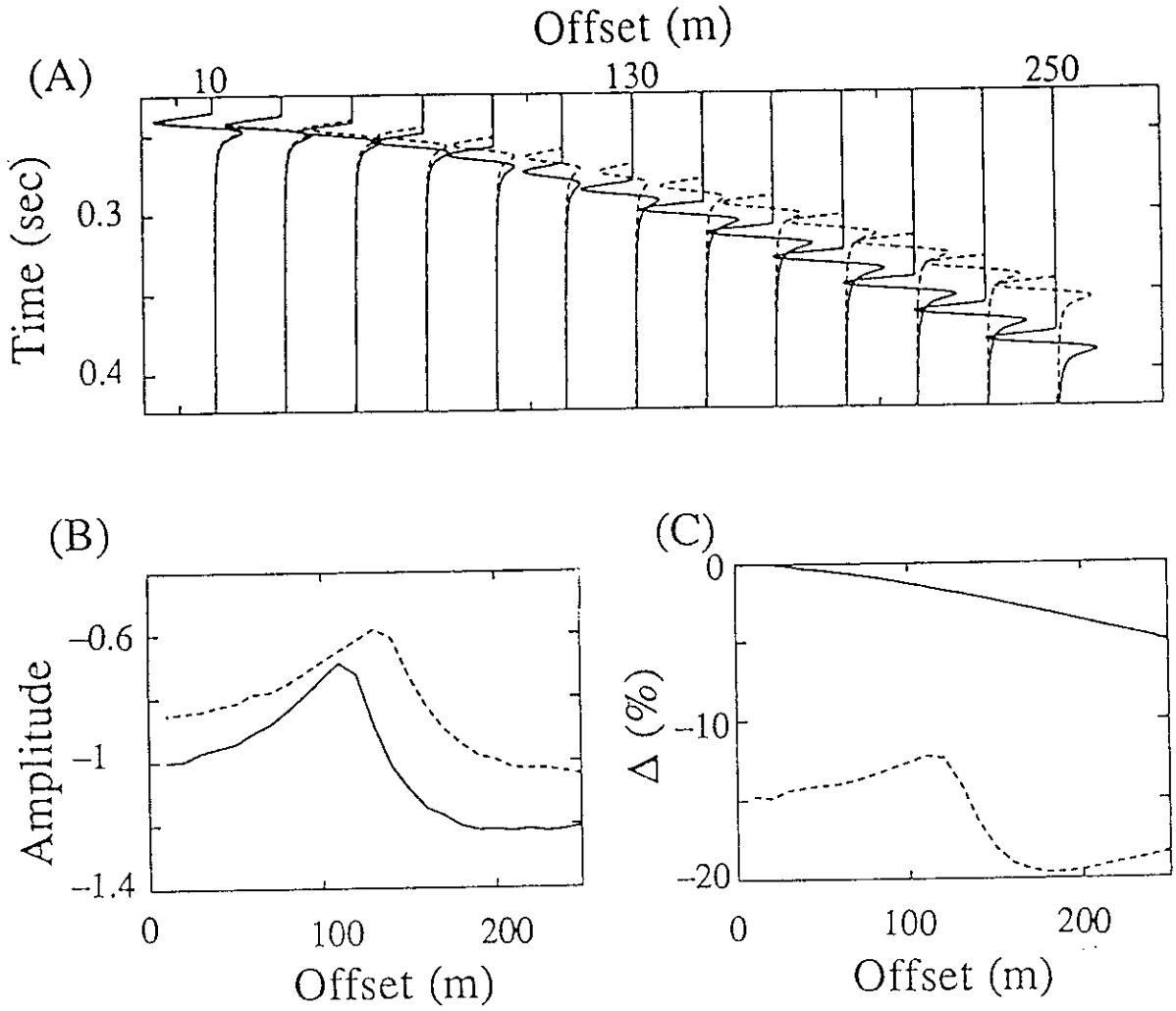

Figure 7: (A) Synthetic reflected amplitudes for a horizontal array of receivers located at the same level as the source (z_o = 100 m, z = – 100 m and Δx = 20 m). The solid curves are for an I/I model: β_1 = 0.85 km/sec and β_2 = 1.7 km/sec. The dashed curves are for a TI/TI model: $(\beta_v)_1$ = 0.85 km/sec, $(\beta_h)_1$ = 1.0 km/sec, $(\beta_v)_2$ = 1.7 km/sec and $(\beta_h)_2$ = 2.0 km/sec. The densities are $\rho_1:\rho_2$ = 1:2. (B) Plot of the reflected amplitudes versus offset for the I/I model (solid) and the TI/TI model (dashed). The amplitudes are scaled by the absolute amplitude of the first trace in the I/I model. (C) The relative change in the arrival times, $\frac{T_{TI/TI} - T_{I/I}}{T_{I/I}}$ (solid) and the reflected amplitudes, $\frac{Amp_{TI/TI} - Amp_{I/I}}{Amp_{I/I}}$ (dashed) versus offset.

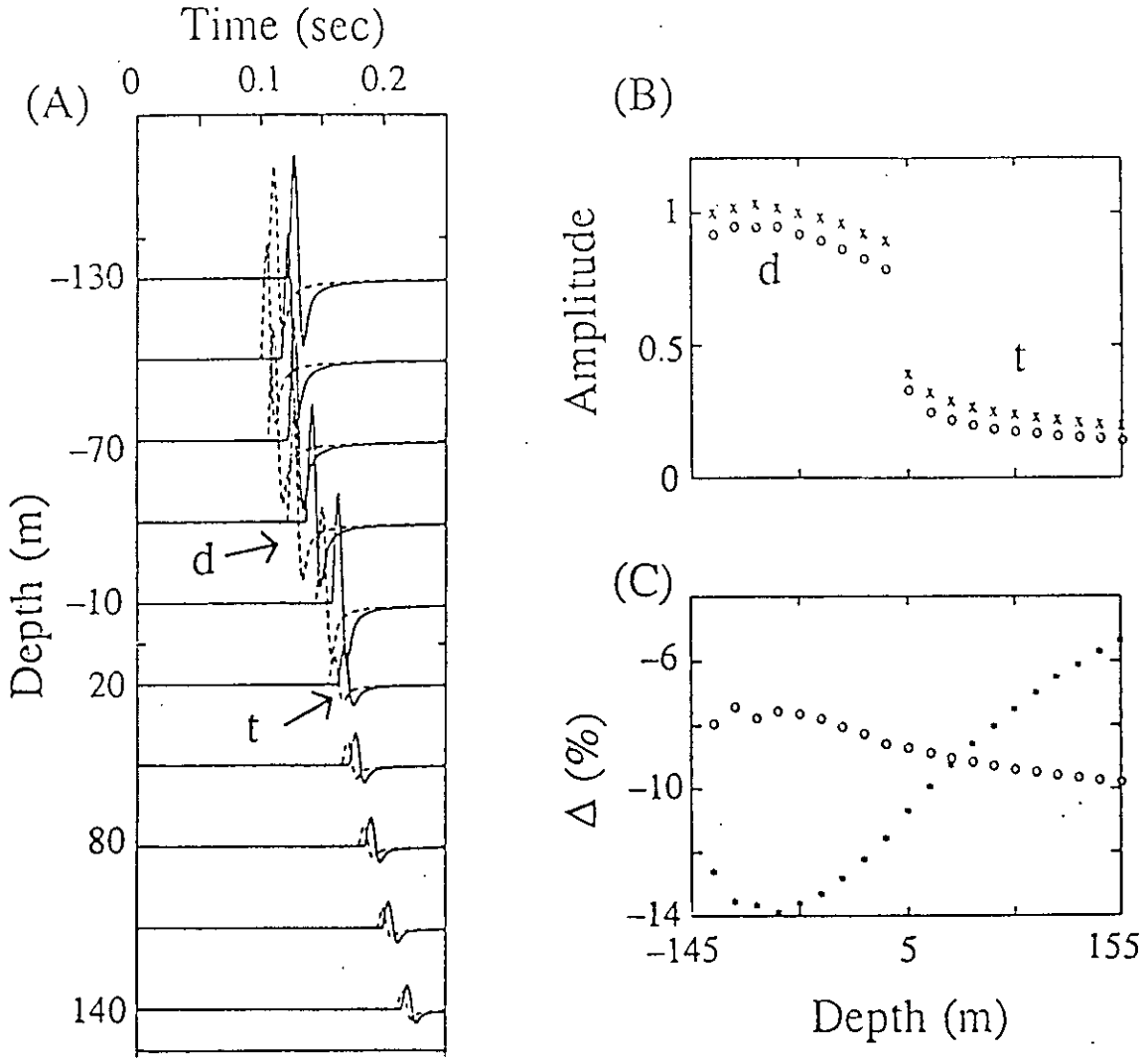

Figure 8: (A) Synthetic seismograms of a vertical seismic profile for an I/I model (solid): β_1 = 0.85 km/sec and β_2 = 1.7 km/sec and a TI/TI model (dashed): $(\beta_v)_1$ = 0.85 km/sec, $(\beta_h)_1$ = 1.0 km/sec, $(\beta_v)_2$ = 1.7 km/sec and $(\beta_h)_2$ = 2.0 km/sec. The densities are $\rho_1:\rho_2$ = 1:2. Only the incident and transmitted arrivals are calculated. The parameters are z_o = 100 m, x = 100 m and Δz = 30 m). (B) Plot of the amplitudes versus depth for the I/I model (crosses) and the TI/TI model (circles). The amplitudes are scaled by the absolute amplitude of the first trace in the I/I model. (C) The relative change in the arrival times, $\frac{T_{TI/TI} - T_{I/I}}{T_{I/I}}$ (stars) and the reflected amplitudes, $\frac{Amp_{TI/TI} - Amp_{I/I}}{Amp_{I/I}}$ (circles) versus depth. The incident and transmitted arrivals are denoted as *(d)* and *(t)* respectively.